Microenvironment and Immunology

Cancer Research

A Threshold Level of Intratumor CD8$^+$ T-cell PD1 Expression Dictates Therapeutic Response to Anti-PD1

Shin Foong Ngiow[1,2], Arabella Young[1,2], Nicolas Jacquelot[3,4,5,6], Takahiro Yamazaki[3,4,5,6], David Enot[3,4,5,6,7], Laurence Zitvogel[3,4,5,6], and Mark J. Smyth[1,2]

Abstract

Despite successes, thus far, a significant proportion of the patients treated with anti-PD1 antibodies have failed to respond. We use mouse tumor models of anti-PD1 sensitivity and resistance and flow cytometry to assess tumor-infiltrating immune cells immediately after therapy. We demonstrate that the expression levels of T-cell PD1 (PD1^{lo}), myeloid, and T-cell PDL1 (PDL1^{hi}) in the tumor microenvironment inversely correlate and dictate the efficacy of anti-PD1 mAb and function of intratumor CD8$^+$ T cells. In sensitive tumors, we reveal a threshold for PD1 downregulation on tumor-infiltrating CD8$^+$ T cells below which the release of adaptive immune resistance is achieved. In contrast, PD1^{hi} T cells in resistant tumors fail to be rescued by anti-PD1 therapy and remain dysfunctional unless intratumor PDL1^{lo} immune cells are targeted. Intratumor Tregs are partly responsible for the development of anti-PD1–resistant tumors and PD1^{hi} CD8$^+$ T cells. Our analyses provide a framework to interrogate intratumor CD8$^+$ T-cell PD1 and immune PDL1 levels and response in human cancer. *Cancer Res; 75(18); 3800–11. ©2015 AACR.*

Introduction

Immune checkpoint molecules refer to a group of immune receptors that when engaged by their ligands, transmit an inhibitory signal to suppress effector function. These inhibitory pathways are critical for maintaining self-tolerance and regulating the strength and duration of immune responses in peripheral tissues to minimize tissue pathology (1). We now appreciate cancer can use these pathways to evade tumor immunity. Three immune checkpoint inhibitor monoclonal antibodies (mAb), ipilimumab [reactive with cytotoxic T lymphocyte-associated protein 4 (CTLA-4)], pembrolizumab, and nivolumab [reactive with programmed death 1 (PD1)], were approved by the FDA for the treatment of advanced melanoma. Anti-CTLA-4 and anti-PD1 are thought to mediate their antitumor activity by blocking CTLA-4 or PD1 on effector immune cells (such as CD8$^+$ T cells) from interacting with their ligands CD80/CD86 or PDL1/PDL2 (programmed death ligand 1/2), respectively (2, 3). Central to the efficacy of immune checkpoint blockade is the requirement for immune cells to infiltrate into tumors.

Owing to recent success in numerous clinical trials and a more favorable clinical safety profile (3–6), anti-PD1 mAb therapy is expected to ascend to be a frontline treatment for advanced melanoma and various other malignancies. Anti-PD1 mAbs were shown to induce variable, but impressive, levels of clinical responses in patients with melanoma, renal cell carcinoma, non–small cell lung cancer (NSCLC), and Hodgkin lymphoma (3–6). Anti-PDL1 therapy also shows considerable promise and more recently was shown to have activity in bladder carcinoma (7). This new survival profile now raises questions about how to predict and increase the number of patients who receive long-term clinical benefit from immune checkpoint mAb therapy. Tumor-infiltrating lymphocytes (TIL) were strongly associated with local PDL1 expression on melanomas (primary or metastases; ref. 8). Tumors and immune cells in tumors upregulate PDL1 in response to IFNγ released by TILs as an adaptive immune resistance mechanism to suppress local effector T-cell function (1), implying that immunosurveillance exists even in advanced cancers. PDL1 can also be expressed constitutively on cancer cells through poorly characterized oncogenic signaling pathways (9–11). Recent studies in patients reported that the presence of tumor CD8$^+$ T cells and PD1 and PDL1 expression are positive predictive biomarkers for anti-PD1 therapy (12). As PD1 expression is generally localized on intratumor T cells (1, 13), it is thus not surprising that a preexisting T-cell response dictates anti-PD1 treatment outcome. By blocking the ligation of PD1 by its ligands, PD1-expressing T cells were demonstrated to have enhanced cytotoxic, proliferation, and migration capacity (13).

Here, we have compared anti-PD1–sensitive and -resistant mouse tumors that paradoxically both contain CD8$^+$ T cells. The expression levels of intratumor T-cell PD1 (^{hi} and ^{lo}) and immune cell PDL1 (^{lo} and ^{hi}) dictated the resistance or sensitivity to anti-PD1 mAb, respectively. In sensitive tumors, we reveal a threshold for PD1 downregulation on tumor-infiltrating T cells below which the release of adaptive immune resistance is achieved. We show

[1]Immunology in Cancer and Infection Laboratory, QIMR Berghofer Medical Research Institute, Herston, Queensland, Australia. [2]School of Medicine, University of Queensland, Herston, Queensland, Australia. [3]INSERM U1015, Villejuif, France. [4]Institut de Cancérologie Gustave Roussy, Villejuif, France. [5]Equipe labellisée Ligue contre le Cancer, University of Paris Sud XI, Villejuif, France. [6]Center of Clinical Investigations in Biotherapies of Cancer (CICBT), Villejuif, France. [7]Metabolomics and Cell Biology Platforms, Institut de Cancerologie Gustave Roussy, Villejuif, France.

Note: Supplementary data for this article are available at Cancer Research Online (http://cancerres.aacrjournals.org/).

Corresponding Author: Mark J. Smyth, QIMR Berghofer Medical Research Institute, 300 Herston Road, Herston 4006, Queensland, Australia. Phone: 61-7-8345-3957; Fax: 61-7-3362-0111; E-mail: mark.smyth@qimrberghofer.edu.au

doi: 10.1158/0008-5472.CAN-15-1082

that an induction of intratumor Treg is, in part, responsible for the development of anti-PD1–resistant tumors and $PD1^{hi}$ $CD8^+$ T cells.

Materials and Methods

Mice

C57BL/6 and Balb/c wild-type (WT) were purchased from the ARC Animal Resources Center or Walter and Eliza Hall Institute for Medical Research. C57BL/6 FcR-deficient ($FcR\gamma^{KO}$, $Fc\gamma R\ III^{KO}$ $Fc\gamma R\ IV^{KO}$; kindly provided by Mark Hogarth and Jeffrey Ravetch, respectively; refs. 14–17) and C57BL/6 Foxp3-DTR transgenic mice (18) were bred in-house at the QIMR Berghofer Medical Research Institute and used between the ages of 6 and 16 weeks. Groups of 4 to 10 mice per experiment were used for experimental tumor assays to ensure adequate power to detect biologic differences. All experiments were approved by the QIMR Berghofer Medical Research Institute Animal Ethics Committee.

Tumor cell lines

The C57BL/6 MC38 colon adenocarcinoma, C57BL/6 AT3 mammary adenocarcinoma, and Balb/c CT26 colon adenocarcinoma were maintained as previously described (19, 20). For *in vivo* experiments, the indicated cell numbers were s.c. injected into mice in a 100-μL volume.

Antibodies and reagents

Purified anti-mouse PD1 mAb (RMP1-14), anti-mouse Tim3 (RMT3-23), anti-mouse PDL1 (10F.9G2), and control Ig (2A3) were purchased from BioXCell and used in the schedule and dose as indicated. Diphtheria toxin (DT) was purchased from Sigma Aldrich (Cat No D0564) and used in the schedule and dose as indicated.

In vivo treatments

A total of 1×10^6 MC38 or AT3 tumor cells and 2×10^5 Renca or 1×10^5 CT26 tumor cells were s.c. injected into mice in a 100-μL volume (day 0) and treatments given as indicated in the figure legends. Tumor growth was measured using a digital caliper, and tumor sizes are presented as mean ± SEM. At indicated time points, tumors were weighed and recorded (mg) for individual mice in each group. For flow cytometric analyses of immune cells (TILs or peripheral lymphoid tissues), MC38 or CT26-bearing mice were treated with the indicated antibodies or reagents on day 10 and immune cells were isolated 48 to 72 hours after treatment; AT3-bearing mice were treated with the indicated antibodies or reagents on day 14 and immune cells were isolated 48 to 96 hours after treatment; Renca-bearing mice were treated with the indicated antibodies or reagents on day 8 and immune cells were isolated 48 hours after treatment. For $Foxp3^+$ Treg depletion, 500 ng of DT (200 μL volume) was intraperitoneally injected in MC38- or AT3-bearing Foxp3-DTR transgenic mice at the indicated time, and an equal volume of PBS was used as a control.

Flow cytometric analysis

Tumors and peripheral lymphoid tissues were harvested from mice that had been treated with mAb or otherwise and processed for flow cytometric analysis as previously described (19). For surface staining, TILs or immune cell suspensions were stained with eFluor780 anti-CD45.2 (104; eBioscience), eFluor450 or BV605 anti-CD4 (RM4-5; eBioscience and Biolegend), PE-Cy7 or BV421 anti-CD8a (53-6.7; eBioscience and Biolegend), FITC, phycoerythrin (PE), or APC anti-TCRβ (H57-597; eBioscience and Biolegend), PE-Cy7 anti-CD11b (M1/70; eBioscience), eFluor450 anti-Gr1 (RB6-8C5; eBioscience), PE anti-CD44 (IM7; Biolegend), APC anti-CD62L (MEL-14; Biolegend), FITC or APC anti-PD1 (J43; eBioscience), APC anti-PDL1 (10F.9G2; Biolegend), and respective isotype antibodies in the presence of anti-CD16/32 (2.4G2). BD Liquid Counting Beads (Cat. No. 335925) were added to sample for cell number analyses. 7AAD (Biolegend) was used to exclude dead cells. For intracellular transcription factor staining, surface-stained cells were fixed and permeabilized using the Foxp3/Transcription Factor Staining Buffer Set (eBioscience), according to the manufacturer's protocol, and stained using eFluor450-anti-Foxp3 (FJK-16s, eBioscience), FITC or PE-Cy7 anti-Tbet (4B10 or eBio4B10; Biolegend and eBioscience), eFluor660 anti-Eomes (Dan11mag; eBioscience), and respective isotype antibodies. For intracellular staining of IFNγ and TNF, cells were stimulated *in vitro* with 50 ng/mL phorbol 12-myristate 13-acetate (PMA; Sigma-Aldrich) and 1 μg/mL ionomycin (Sigma-Aldrich) in the presence of Golgi Plug (BD Biosciences) for 4 hours and then surface stained as aforementioned. Surface-stained cells were then fixed and permeabilized using BD Cytofix/Cytoperm (BD Biosciences) according to the manufacturer's protocol and stained with PE-anti-IFNγ (XMG1.2; eBioscience) and BV605 anti-TNF (MP6-XT22; Biolegend) and respective isotype antibodies. Cells were acquired on the BD FACSCANTO II (BD Biosciences) and analysis was conducted using FlowJo (Tree Star).

Statistical analyses

Statistical analyses were conducted using GraphPad Prism software. Significant differences in tumor growth were determined by an unpaired *t* or Mann–Whitney *U* test. Significant differences in cell subsets were determined by an unpaired *t* test. Analysis of covariance (ANCOVA) was applied to test the association between the PDL1 or PD1 mean fluorescence intensity (MFI) on various TIL subsets ($CD4^+$ T, $CD8^+$ T, $CD11b^+/Gr1^+$, $CD45.2^-$) and the tumor weight and the interaction between the 2 slopes. Values of $P < 0.05$ were considered significant.

Results

Anti-PD1 sensitivity correlates with reduced frequency of PD1-expressing T cells

We set out to compare the intratumor effects of anti-mouse PD1 therapy in sensitive and resistant mouse tumors where $CD8^+$ T cells were prominent. Here, we chose the sensitive MC38 colon adenocarcinoma and resistant AT3 mammary tumor models. Consistent with our published data, anti-PD1 suppressed the growth and weight of MC38 (19), but not AT3 (20), tumors in comparison to the control cIg-treated mice (Fig. 1A and B; Supplementary Fig. S1A and S1C). We next performed flow cytometric analyses on TILs 48 to 72 hours after one mAb treatment and used a noncompeting clone of anti-PD1 mAb (clone J43) for flow cytometric staining analysis (Supplementary Fig. S2). Both MC38 and AT3 tumors contain a similar high frequency and number of leukocytes ($CD45.2^+$) and T cells ($CD4^+$ and $CD8^+$). While we did not observe significant changes in the intratumor leukocyte ($CD45.2^+$) number and frequency between anti-PD1- and cIg-treated mice, anti-PD1 mAb induced a modest increase in the frequency and number of $CD8^+$ T cells in MC38 tumors, but not

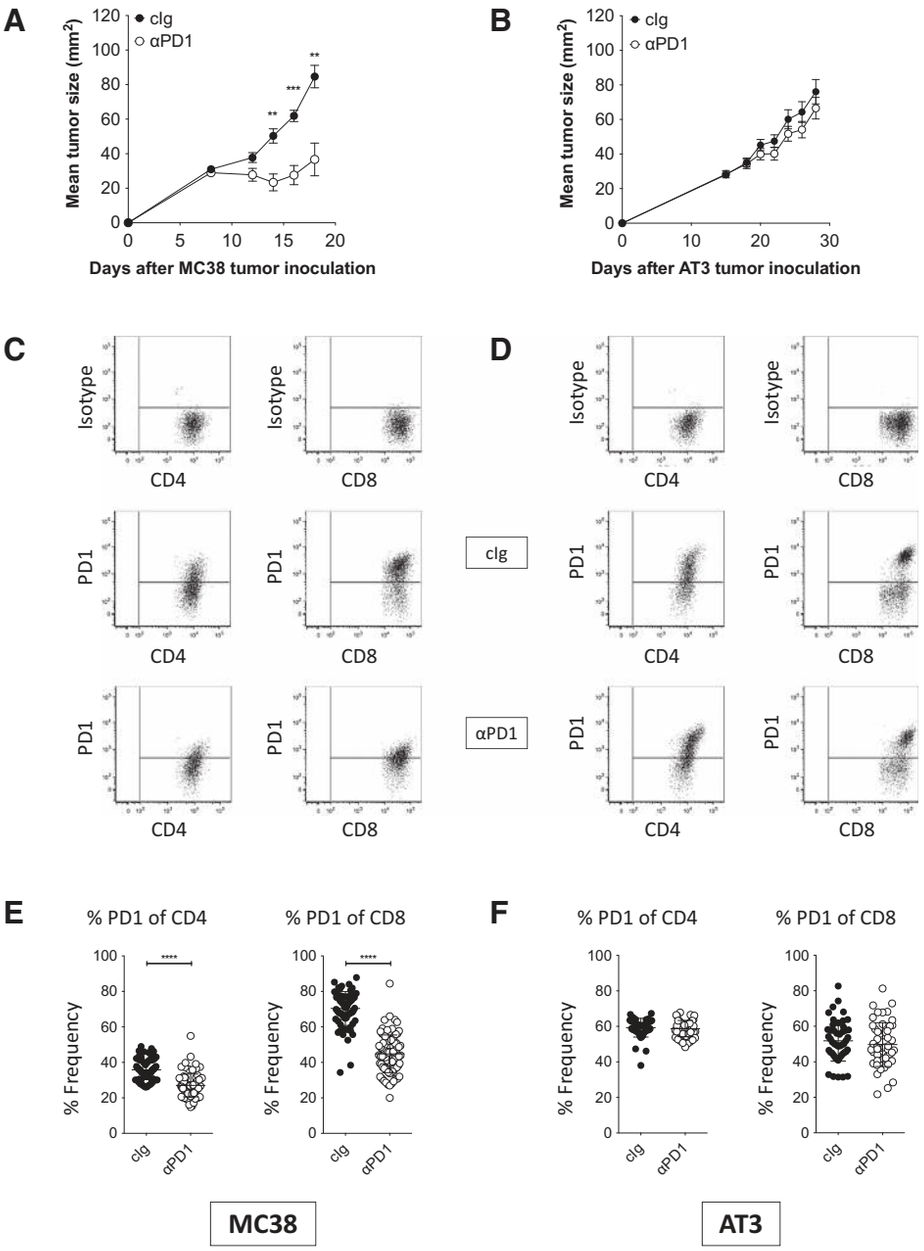

Figure 1.
Anti-PD1 sensitivity correlates with reduced frequency of PD1-expressing $CD8^+$ T cells. Groups of B6 WT mice ($n = 5$–8) were s.c. injected with MC38 tumor (1×10^6 cells; A, C, and E) or AT3 tumor (1×10^6 cells; B, D, and F) on day 0. A and B, tumor-bearing mice were treated with 250 μg of cIg or anti-PD1 on days 6, 10, and 14 (A) or days 15, 19, 23, and 27 (B). Tumor growth was measured using a digital caliper, and tumor sizes are presented as mean ± SEM. Statistical differences in tumor sizes between cIg- and anti-PD1–treated mice were determined by an unpaired *t* test (**, $P < 0.01$; ***, $P < 0.001$). Data are representative of two or more independent experiments. C–F, tumor-bearing mice were treated with 250 μg of cIg or anti-PD1 on day 10 (C and E) or day 14 (D and F), and tumors were harvested 2 or 3 days after antibody treatments for flow cytometric analyses. C and D, representative FACS plots for gating strategy to define frequencies of PD1-expressing $CD4^+$ T cells (left) and $CD8^+$ T cells (right) between cIg- and anti-PD1–treated mice are shown. E and F, frequencies of PD1-expressing $CD4^+$ T cells and $CD8^+$ T cells are shown. Statistical differences in frequencies of PD1-expressing $CD4^+$ T cells and $CD8^+$ T cells between cIg- and anti-PD1–treated mice were determined by an unpaired *t* test (****, $P < 0.0001$). Data shown are pooled from 12 (E) and 7 (F) independent experiments and are presented as the mean ± SD, with individual symbols representing individual mice. Data shown for frequencies of PD1-expressing $CD4^+$ T cells, and PD1-expressing $CD8^+$ T cells between cIg- and anti-PD1–treated mice (E and F) are the same data set as shown in Supplementary Fig. S1B and S1D.

AT3 tumors (Supplementary Fig. S1B and S1D). In contrast, intratumor $CD4^+$ T-cell number and frequency were moderately increased after anti-PD1 treatment compared with cIg treatment in both tumor models (Supplementary Fig. S1B and S1D).

The frequency of intratumor T cells expressing PD1 was calculated relative to isotype control–stained cells (Fig. 1C and D). Strikingly, the intratumor frequency of PD1-expressing $CD8^+$ and $CD4^+$ T cells was significantly reduced in MC38 tumors, but not AT3 tumors, following anti-PD1 treatment (Fig. 1E and F; Supplementary Fig. S1B and S1D). In contrast, we observed that the PD1 expression levels were decreased in both $CD4^+$ and $CD8^+$ T cells in MC38 and AT3 tumors after anti-PD1 treatment compared with cIg treatment, indicating the biologic, if not therapeutic, activity of anti-PD1 in each tumor model (Supplementary Fig. S3). Notably, intratumor $CD4^+$ and $CD8^+$ T cell PD1 expression was higher in AT3 tumors than in MC38 tumors, with two clear populations of $PD1^{hi}$ and $PD1^-$ $CD8^+$ T cells in AT3 tumors and a relatively homogenous $PD1^{lo}$-expressing population of $CD8^+$ T cells in MC38 tumors (hereafter termed $PD1^{lo}$; Fig. 1C and D; Supplementary Fig. S3). Of note, these $PD1^{hi}$ (AT3) and $PD1^{lo}$ (MC38) $CD8^+$ T cells existed before cIg or anti-PD1 is given (data not shown). Collectively, these data indicated a strong association between the presence of intratumor $PD1^{hi}$ T cells and resistance to anti-PD1 mAb. However, just as importantly, a significant reduction in the frequency of $PD1^+$ T cells and level of PD1 expression below a threshold level (as seen in MC38) predicts the release from adaptive immune resistance. The same effects observed in the AT3 model ($PD1^{hi}$ $CD8^+$ T cells associated

with resistance to anti-PD1 mAb and no reduced frequency of $CD8^+$ T cell PD1-expressing cells after anti-PD1 mAb) were also seen in the Renca renal cell carcinoma tumor model (Supplementary Fig. S4).

We further confirmed our findings using a combination of anti-Tim3 and anti-PD1 mAbs in the CT26 tumor model, where a synergistic antitumor response of the combination was previously observed (19). The combination of anti-Tim3 and anti-PD1 mAbs induced a reduction in $PD1^+$ intratumor $CD8^+$ T cells consistent with the ability of anti-Tim3 to enhance an antitumor immune response toward CT26 via anti-PD1 therapy (Supplementary Fig. S5A and S5B). In contrast, consistent with no reduction in $PD1^+$ T cells after the combination treatment of AT3 tumors (Supplementary Fig. S5C), anti-Tim3 and anti-PD1 mAb combination therapy was unable to suppress AT3 tumor growth (Supplementary Fig. S5D).

Blockade of T-cell PD1 determines anti-PD1 activity

The analyses of endpoint tumors reported in numerous studies have shown that anti-PD1 increased the intratumor CD8/Treg ratio (21, 22), and PD1 is expressed on intratumor Treg (23). Given that the antitumor activity of mAb targeting mouse T-cell checkpoint protein (CTLA-4) was reportedly mediated via an Fc-dependent intratumor Treg depletion mechanism (24–26), we next assessed antitumor activity of anti-PD1 in various FcR-deficient mice. Distinct from anti-CTLA-4, anti-PD1 retained its antitumor effect against MC38 in all 3 FcR-deficient strains of mice used compared with WT mice (Supplementary Fig. S6A). Furthermore, our flow cytometric analyses of TILs and peripheral lymphoid tissues [tumor, draining lymph nodes (DLN), non-DLN, spleen, and blood] showed that PD1-expressing T cells were predominantly found in the tumor microenvironment (Supplementary Fig. S7A and S7B). In addition, we did not observe a significant reduction in intratumor T-cell numbers between anti-PD1–treated and cIg-treated mice (Supplementary Fig. S1B and S1D). These data suggested that blockade of PD1 signaling in intratumor T cells is the primary mechanism of action for this anti-PD1 mAb.

Functions of MC38 and AT3 intratumor T cells

We observed that MC38 intratumor T cells produced relatively higher levels of IFNγ and TNF after cIg treatment compared with the T cells isolated from AT3 tumors (Fig. 2A–D). Moreover, we also observed an increase in intratumor T-cell–derived IFNγ, but not TNF, in MC38-bearing mice after anti-PD1 treatment (Fig. 2A and B). In contrast, no significant changes were observed in the intratumor T cell–derived IFNγ and TNF between cIg- and anti-PD1–treated AT3-bearing mice (Fig. 2C and D). Anti-PD1 mAb was shown to increase the Tbet (Fig. 2E), but not Eomes (Fig. 2F), expression in T cells isolated from the MC38 tumors. In contrast, no significant changes were observed for Tbet and Eomes expression levels between cIg- and anti-PD1–treated AT3-bearing mice (Fig. 2G and H). The majority (>85%) of intratumor T cells in both tumor models were found to be $CD44^+CD62L^-$, indicating that differences in their PD1 status were independent of their T-cell activation status (Fig. 3A–D). While anti-PD1 mAb did not modulate the frequencies of $CD44^+CD62L^-$ and $CD44^+CD62L^+$ intratumor T cells in the MC38 tumors (Fig. 3A and B), it marginally reduced the frequency of $CD44^+CD62L^-$ $CD4^+$ T cells in the AT3 tumors (Fig. 3C). Taking all the T-cell parameters that we assessed, our data showed that T-cell PD1 reflects their dysfunctional cytokine production, independent of their activation status.

Anti-PD1 mAb modulates the AT3 CD8/Treg ratio

It has been recently suggested that the presence of Treg could promote the exhaustion of $CD8^+$ T cells (23, 27). However, the role of Treg in regulating T-cell PD1 expression has not been examined. Increases in intratumor $CD4^+$ T cells in both the MC38 and AT3 tumors after administration of anti-PD1 (Supplementary Fig. S1B and S1D) prompted us to assess the proportion of intratumor Treg ($CD4^+Foxp3^+$). Our flow cytometric analyses of TILs showed that intratumor Treg were increased in both tumor models, within 48 to 72 hours after anti-PD1 mAb compared with cIg (Fig. 4A and B). Notably, we found that anti-PD1 mAb significantly reduced the intratumor CD8/Treg ratio in AT3-bearing mice (Fig. 4B). In contrast, this ratio was unchanged between cIg- and anti-PD1–treated MC38-bearing mice (Fig. 4A). To assess the role of Treg in modulating intratumor T-cell PD1, we used a Foxp3-DTR transgenic mouse model to conditionally deplete Treg in both the MC38 and AT3 tumor models. Whereas PD1-expressing $CD8^+$ T cells were unchanged between PBS- and DT-treated mice, we found that Treg depletion increased the PD1-expressing $CD4^+$ T cells in MC38 tumor–bearing mice (Fig. 4C). PD1-expressing T cells isolated from the Treg-depleted AT3 tumor were reduced compared with the Treg-intact controls, and these T cells displayed a significantly lower PD1 expression ($PD1^{hi}$ to $PD1^{lo}$), together with a reduced frequency in $PD1^+$ T cells (Fig. 4E). Of note, these changes in T-cell PD1 were independent of the induction of Tbet (Fig. 4D and F; ref. 28). On the basis of our prediction of anti-PD1 sensitivity, we speculate that these $PD1^{lo}$ T cells are sensitive to anti-PD1 treatment. Consistent with this observation, Treg depletion in AT3 and CT26 renders the tumor sensitive to anti-PD1 (Fig. 4G and H).

Intratumor immune PDL1 and T cell PD1 cross-regulate

Given the constant interaction of PD1 with PDL1 in the tumor microenvironment, we next sought to determine whether T-cell PD1 expression was affected by intratumor PDL1 levels. Our MC38 TIL flow cytometric analyses revealed that PDL1 expression on intratumor T cells and myeloid cells ($CD11b^+$ $Gr1^{hi}$, $CD11b^+$ $Gr1^{int}$, and $CD11b^+$ $Gr1^{lo}$) was significantly increased upon the administration of anti-PD1 mAb (Fig. 5A). Similar increases were also observed in the AT3 tumor model (Fig. 5B). Interestingly, the PDL1 expression on $CD45.2^-$ cells was not different between cIg- and anti-PD1–treated mice in both tumor models (Fig. 5A and B). More importantly, we found that PDL1 expression in all the immune cell subsets analyzed was generally higher in MC38 tumors than in AT3 tumors (Fig. 5A and B). The relatively lower level of PDL1 in the AT3 tumor suggested the use of anti-PDL1 mAb might be an effective therapeutic approach to treat this anti-PD1–resistant tumor, enabling maximal disruption of the PD1/PDL1 axis. We found that anti-PD1 and anti-PDL1 alone were similar in suppressing the growth of MC38, and the combination of both mAbs had an insignificant effect (Fig. 5C). Strikingly, anti-PDL1 mAb was shown to suppress the growth of the AT3 tumor (Fig. 5D). Similar to MC38 tumors, AT3-bearing mice administered with the combination of anti-PD1 and anti-PDL1 mAbs did not result in any measurable additive antitumor effect in comparison to anti-PDL1 mAb alone (Fig. 5D). Like anti-PD1 mAb, the antitumor activity of anti-PDL1 mAb was FcRγ-independent (Supplementary Fig. S6B).

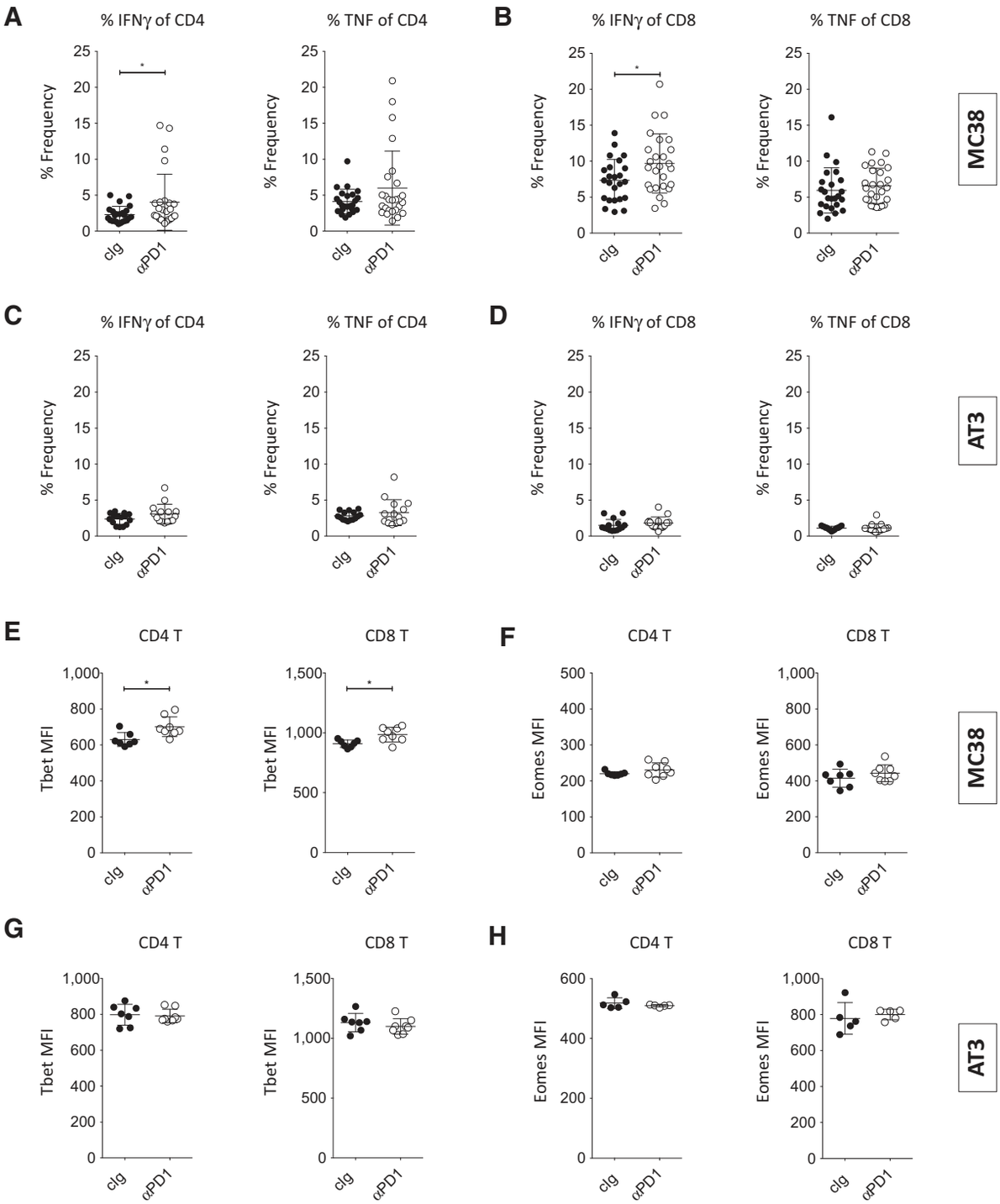

Figure 2.

Anti-PD1 mAb sensitivity correlates with intratumor T-cell inflammatory cytokines. Groups of B6 WT mice ($n = 5$–8) were s.c. injected with MC38 tumor (1×10^6 cells; A, B, E, and F) or AT3 tumor (1×10^6 cells; C, D, G, and H) on day 0. Tumor-bearing mice were treated with 250 μg of cIg or anti-PD1 on day 10 (A, B, E, and F) or day 14 (C, D, G, and H), and tumors were harvested 2 or 3 days after antibody treatments for flow cytometric analyses. A–D, frequencies of IFNγ- and TNF-expressing $CD4^+$ T cells (A and C) and $CD8^+$ T cells (B and D) between cIg- and anti-PD1–treated mice are shown. Data are presented as the mean ± SD, with individual symbols representing individual mice. Statistical differences in frequencies of IFNγ- and TNF-producing cells of $CD4^+$; and $CD8^+$ T-cell subsets between cIg- and anti-PD1–treated mice were determined by an unpaired *t* test (*, $P < 0.05$). Data shown are representative of three (A and B) and two (C and D) independent experiments. Tbet MFI (E and G) and Eomes MFI (F and H) of $CD4^+$ T cells and $CD8^+$ T cells between cIg- and anti-PD1–treated mice are shown. Data are presented as the mean ± SD, with individual symbols representing individual mice. Statistical differences in Tbet MFI (E and G) and Eomes MFI (F and H) of $CD4^+$ and $CD8^+$ T-cell subsets between cIg- and anti-PD1–treated mice were determined by an unpaired *t* test (* $P < 0.05$). Data shown are representative of four or more (E and F) and three (G and H) independent experiments.

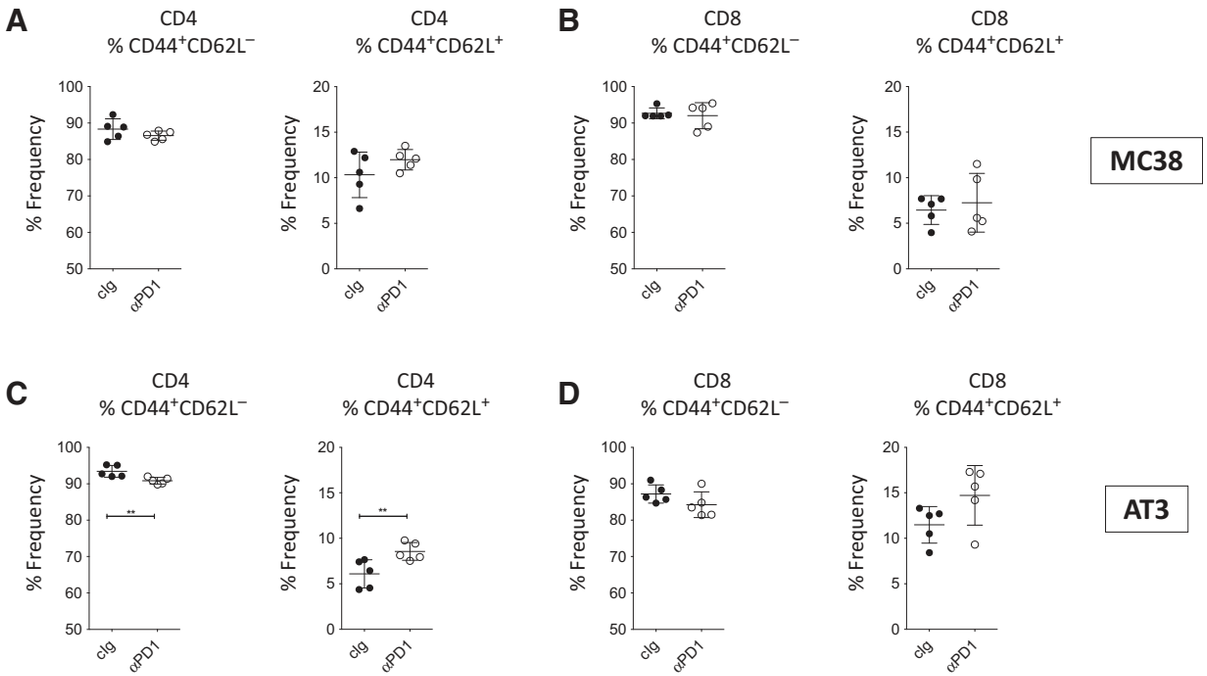

Figure 3.

T-cell PD1 level and frequency is independent of T-cell differentiation. Groups of B6 WT mice ($n = 5$–8) were s.c. injected with MC38 tumor (1×10^6 cells; A and B) or AT3 tumor (1×10^6 cells; C and D) on day 0. Tumor-bearing mice were treated with 250 μg of cIg or anti-PD1 on day 10 (A and B) or day 14 (C and D), and tumors were harvested 2 or 3 days after antibody treatments for flow cytometric analyses. Frequencies of $CD44^+CD62L^-$ and $CD44^+CD62L^+$ in $CD4^+$ T cells (A and C) and $CD8^+$ T cells (B and D) between cIg- and anti-PD1–treated mice are shown. Data are presented as the mean ± SD of 5 mice, with individual symbols representing individual mice. Statistical differences in the frequencies of $CD44^+CD62L^-$ and $CD44^+CD62L^+$ in $CD4^+$ and $CD8^+$ T-cell subsets between cIg- and anti-PD1–treated mice were determined by an unpaired *t* test (**, $P < 0.01$). Data shown are representative of four (A and B) and two (C and D) independent experiments.

Hierarchical model of TIL subset PD1 and PDL1 expression

We next performed an ANCOVA aimed at testing the association between the mean fluorescence intensity of each variable and the tumor weight (measured at 48 to 72 hours after mAb administration) as well as the interactions between the slopes of the treatment groups. The MFI of PD1 expression on T cells and the PDL1 expression on $CD4^+$ T cells are the most significant parameters associated with tumor progression only in MC38 tumors (Fig. 6A, B, and E). Indeed, these variables on total $CD4^+$ and $CD8^+$ T cells do not have any prognostic value in AT3 tumors (Fig. 6C, D, G, and H). Importantly, the high MFI of PD1 expression on T cells lost its negative prognostic value during PD1 blockade therapy (Fig. 6A and B; $P_{\text{interaction}} = 0.001$ for CD8 T, $P_{\text{interaction}} = 0.01$ for CD4 T). Moreover, lower levels of PDL1 expression on $CD8^+$ TILs are predicting responses to anti-PD1 mAb (Fig. 6F). In the resistant AT3 tumors, lower expression of PDL1 on total $CD8^+$ TILs was the only parameter associated with relative tumor indolence (Fig. 6H), likely accounting for the efficacy of anti-PDL1 Ab in this model (Fig. 5D). Given the presence of $PD1^-$ and $PD1^{hi}$ $CD8^+$ T cells in AT3 tumors, we also performed the ANCOVA analysis on the selected $CD8^+$ T-cell subsets. While the PD1 MFI prognostic value of MC38 $CD8^+$ T cells was retained (Supplementary Fig. S8A and 8C), we found that AT3 $CD8^+$ $PD1^-$ or $PD1^{hi}$ T cell PD1 MFI did not demonstrate a correlation to tumor progression (Supplementary Fig. S8C and S8D). Surprisingly, we found a positive correlation between PD1 MFI levels and tumor progression in anti-PD1–treated AT3 tumors (Supplementary Fig. S8C and S8D). These data also suggested an induction of PD1 expression on $CD8^+$ T cells is a potential resistance mechanism to anti-PD1 mAb therapy in AT3 tumors. Of note, the MFI of PDL1 on various myeloid cell subsets or $CD45.2^-$ fractions did not retain significant prognostic or predictive value in this interactive model (data not shown).

Discussion

By analyzing patients treated with anti-human PD1 (pembrolizumab or nivolumab), it has been recently shown that preexisting intratumor $PD1^+$ $CD8^+$ T cells, together with the presence of PDL1-expressing cells in the tumor microenvironment, are biomarkers that positively predict response to anti-PD1 mAb therapy (3, 12). While this is a significant step forward, a greater interrogation of both mouse models and patient-derived material may lead to an even more sophisticated understanding. We now appreciate from studying mouse models of anti-PD1 sensitivity and resistance, immediately after anti-PD1 therapy, that the levels of intratumor PD1 on T cells and PDL1 on immune cells (mainly T cells) are critical parameters. We have found that the presence of intratumor $PD1^{lo}$ T cells at the time of anti-PD1 treatment; and a reduction in the frequency of intratumor $PD1^+$ T cells after the administration of anti-PD1 positively predict response. In contrast, anti-PD1–insensitive tumors were infiltrated with $PD1^{hi}$ T cells and did not alter in the frequency of intratumor $PD1^+$ T cells after anti-PD1 mAb therapy. Our flow cytometric analyses of TILs

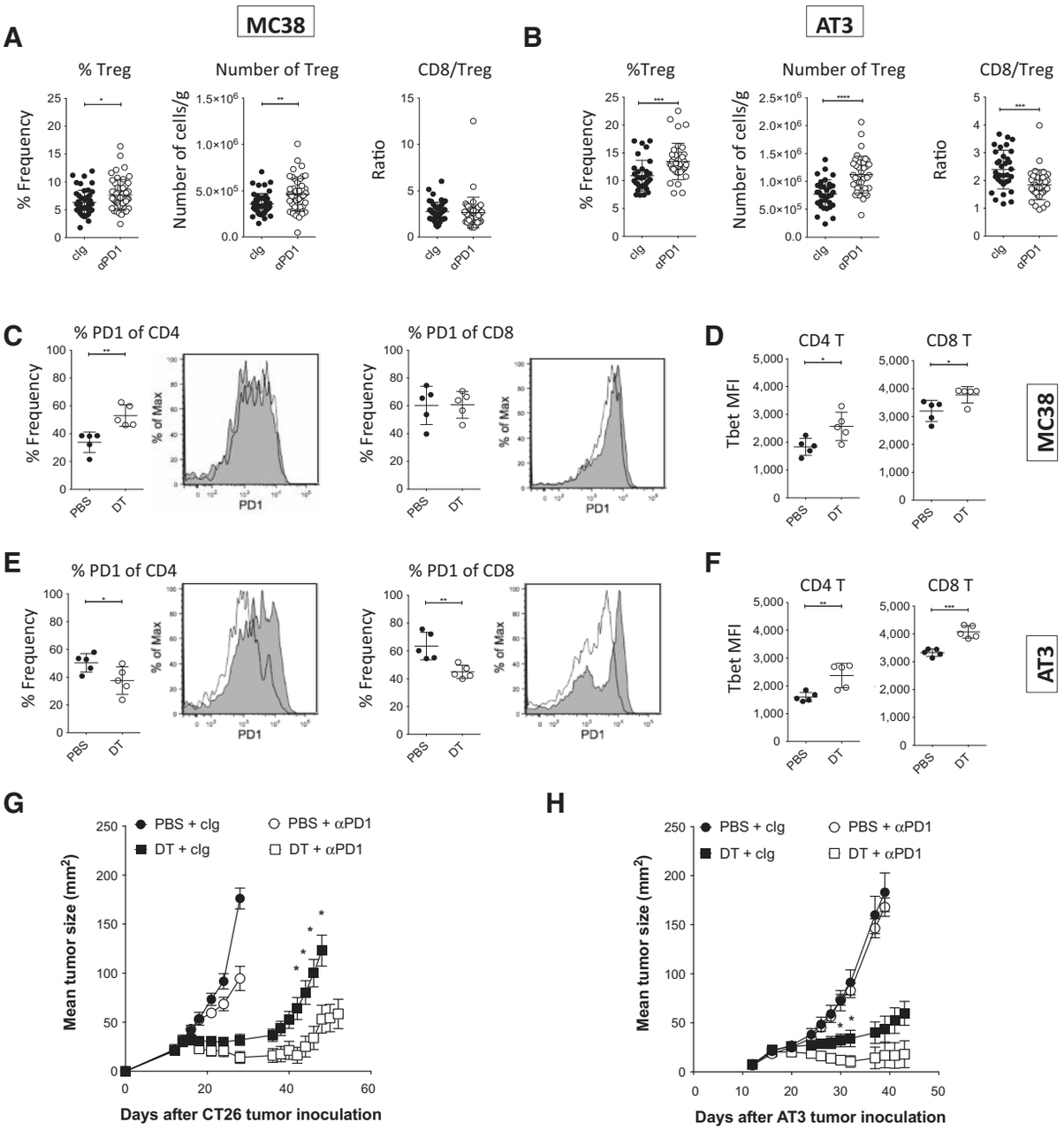

Figure 4.

Treg promotes anti-PD1–resistant PD1^{hi} T cells. Groups of B6 WT (A and B) and Foxp3-DTR (C–F) mice ($n = 5$–10) were s.c. injected with MC38 tumor (1×10^6 cells; A, C, and D) or AT3 tumor (1×10^6 cells; B, E, and F) on day 0. A and B, tumor-bearing mice were treated with 250 μg of clg or anti-PD1 on day 10 (A) or day 14 (B), and tumors were harvested 2 or 3 days after antibody treatments for flow cytometric analyses. Frequencies, numbers of Treg (CD4$^+$Foxp3$^+$), and CD8/Treg ratio between clg- and anti-PD1–treated mice are shown. Data are presented as the mean ± SD, with individual symbols representing individual mice. Statistical differences in the frequencies, cell numbers, and CD8/Treg ratio between clg- and anti-PD1–treated mice were determined by an unpaired *t* test (*, $P < 0.05$; **, $P < 0.01$; ***, $P < 0.001$; ****, $P < 0.0001$). Data shown are pooled from 7 (A) and 5 (B) independent experiments. C–F, tumor-bearing Foxp3-DTR mice were treated with PBS or 500 ng of DT on day 10 (C and D) or day 14 (E and F), and tumors were harvested 3 or 4 days after PBS/DT treatment for flow cytometric analyses. C and E, frequencies of PD1-expressing CD4$^+$ and CD8$^+$ T cells with their representative histogram plots (shaded histogram, PBS-treated; open histogram, DT-treated) from PBS- and DT-treated mice are shown. Data are presented as the mean ± SD with individual symbols representing individual mice. D and F, Tbet MFI of CD4$^+$ and CD8$^+$ T cells of PBS- and DT-treated mice are shown. Data are presented as the mean ± SD, with individual symbols representing individual mice. Statistical differences in frequencies of PD1-expressing T cells (C and E) and Tbet MFI (D and F) of respective cell subsets between PBS- and DT-treated mice were determined by an unpaired *t* test (*, $P < 0.05$; **, $P < 0.01$; ***, $P < 0.001$). G and H, groups of Balb/c or B6 Foxp3-DTR mice ($n = 5$) were s.c. injected with CT26 tumor (1×10^5 cells; G) or AT3 tumor (5×10^5 cells; H) on day 0. G, CT26-bearing mice were treated PBS or 250 ng DT on day 14 as indicated. Mice then received 250 μg of clg or anti-PD1 on days 17, 20, and 22. H, AT3-bearing mice were treated with PBS or 100 ng DT on day 16 as indicated. Mice then received 250 μg of clg or anti-PD1 on days 20, 24, and 28. Tumor growth was measured using a digital caliper, and tumor sizes are presented as mean ± SEM. Statistical differences in tumor growth between DT- and DT and anti-PD1–treated mice were determined by a Mann–Whitney test (*, $P < 0.05$).

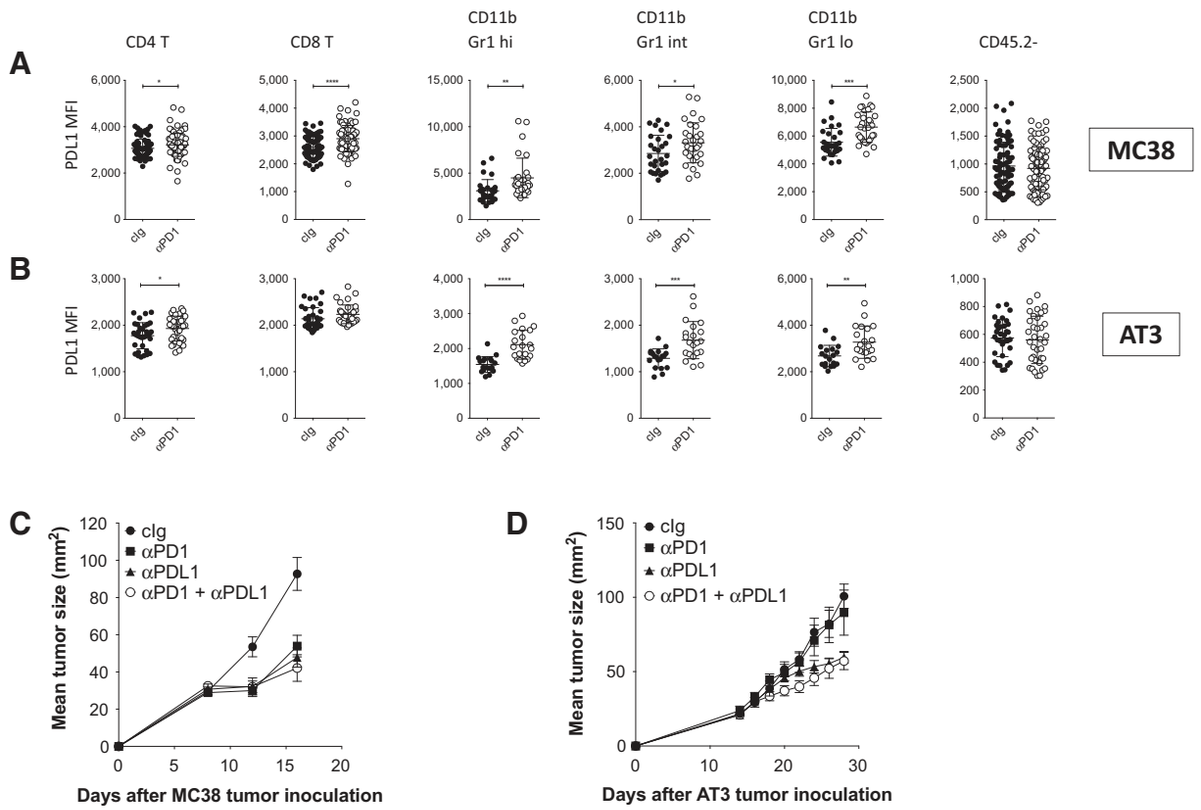

Figure 5.

Anti-PDL1 mAb suppresses anti-PD1–resistant tumor. Groups of B6 WT mice ($n = 5$-8) were subcutaneously injected with MC38 tumor (1×10^6 cells; A and C) or AT3 tumor (1×10^6 cells; B and D) on day 0. A and B, tumor-bearing mice were treated with 250 μg of cIg or anti-PD1 on day 10 (A) or day 14 (B), and tumors were harvested 2 or 3 days after antibody treatments for flow cytometric analyses. PDL1 MFI of $CD4^+$ T cells, $CD8^+$ T cells, CD11b $Gr1^{hi}$ cells, CD11b $Gr1^{int}$ cells, CD11b $Gr1^{lo}$ cells, $CD45.2^-$ cells ($7AAD^-$ $CD45.2^-$) between cIg- and anti-PD1–treated mice are shown. Statistical differences in PDL1 MFI of indicated cell subsets between cIg- and anti-PD1–treated mice were determined by an unpaired *t* test (*, $P < 0.05$; **, $P < 0.01$; ***, $P < 0.001$; ****, $P < 0.0001$). Data shown are pooled from 5 or more (A) and three or more (B) independent experiments. C and D, tumor-bearing mice were treated with 250 μg of cIg, anti-PD1, and/or anti-PDL1 on days 8, 12, and 16 (C) or days 14, 18, 22, and 26 (D). Tumor growth was measured using a digital caliper, and tumor sizes are presented as mean ± SEM. Statistical differences in tumor sizes between cIg-, anti-PD1-, anti-PDL1-, and anti-PD1 + anti-PDL1–treated mice were determined by an unpaired *t* test (day 16 MC38: cIg vs. anti-PD1 $P = 0.0035$; cIg vs. anti-PDL1 $P = 0.0010$; cIg vs. anti-PD1 + PDL1, $P = 0.0006$; day 28 AT3: cIg vs. anti-PDL1, $P = 0.0008$; cIg vs. anti-PD1 + anti-PDL1, $P = 0.0007$). Data are representative of two independent experiments. Tumor growth data for cIg- and anti-PD1–treated mice shown in D are the same dataset as shown in Supplementary Fig. S5D.

showed that anti-PD1 mAb downregulated the PD1 expression on intratumor T cells in both sensitive and resistant tumors but that a certain threshold for the PD1 downregulation had to be achieved for the release of adaptive immune resistance. Consequently, $PD1^{hi}$ T cells in resistant tumors failed to be rescued by anti-PD1 therapy and remained dysfunctional unless intratumor $PDL1^{lo}$ immune cells were targeted. Our study provides a new framework to examine intratumor T-cell PD1 and immune PDL1 levels in human cancer patients with intratumor $CD8^+$ T cells and a view to predicting patient responsiveness to anti-PD1/PDL1 therapies.

We demonstrated that induction of intratumor Treg was, in part, a mechanism responsible for the development of anti-PD1–resistant tumors and $PD1^{hi}$ $CD8^+$ T cells. We reasoned that the induction of Treg and/or increased PDL1 expression within the tumor microenvironment might be adaptive immune resistance mechanisms to counteract the immune activation elicited by PD1 blockade on T cells. An increased expression of CTLA-4 after anti-PDL1 (MPDL3280A) treatment was also suggested to be a positive predictive biomarker in patients (29). In concordance with the expression of CTLA-4 by Treg, we showed that Treg were induced in anti-PD1–treated MC38-bearing hosts. However, the induction of Treg was not restricted to the anti-PD1–sensitive MC38 tumor model, as we observed an even higher number of Treg being induced in the AT3 tumor after the administration of anti-PD1 mAb. Furthermore, our data also revealed that a reduced CD8/Treg ratio (an immune signature generally associated with immune escape) could be used as a negative predictive biomarker for anti-PD1 treatment. Importantly, we demonstrated that in the absence of Treg, $PD1^{hi}$ T cells were converted to $PD1^{lo}$ T cells, enabling increased sensitivity to anti-PD1 treatment. Notably, unlike anti-CTLA-4, anti-PD1 mAb was not Treg-depleting, but rather FcR- independent in its antitumor activity. In this light, our data suggested that anti-PD1–insensitive tumors could be rendered anti-PD1–sensitive by reducing or depleting intratumor Treg. We speculate that the synergistic antitumor effect observed

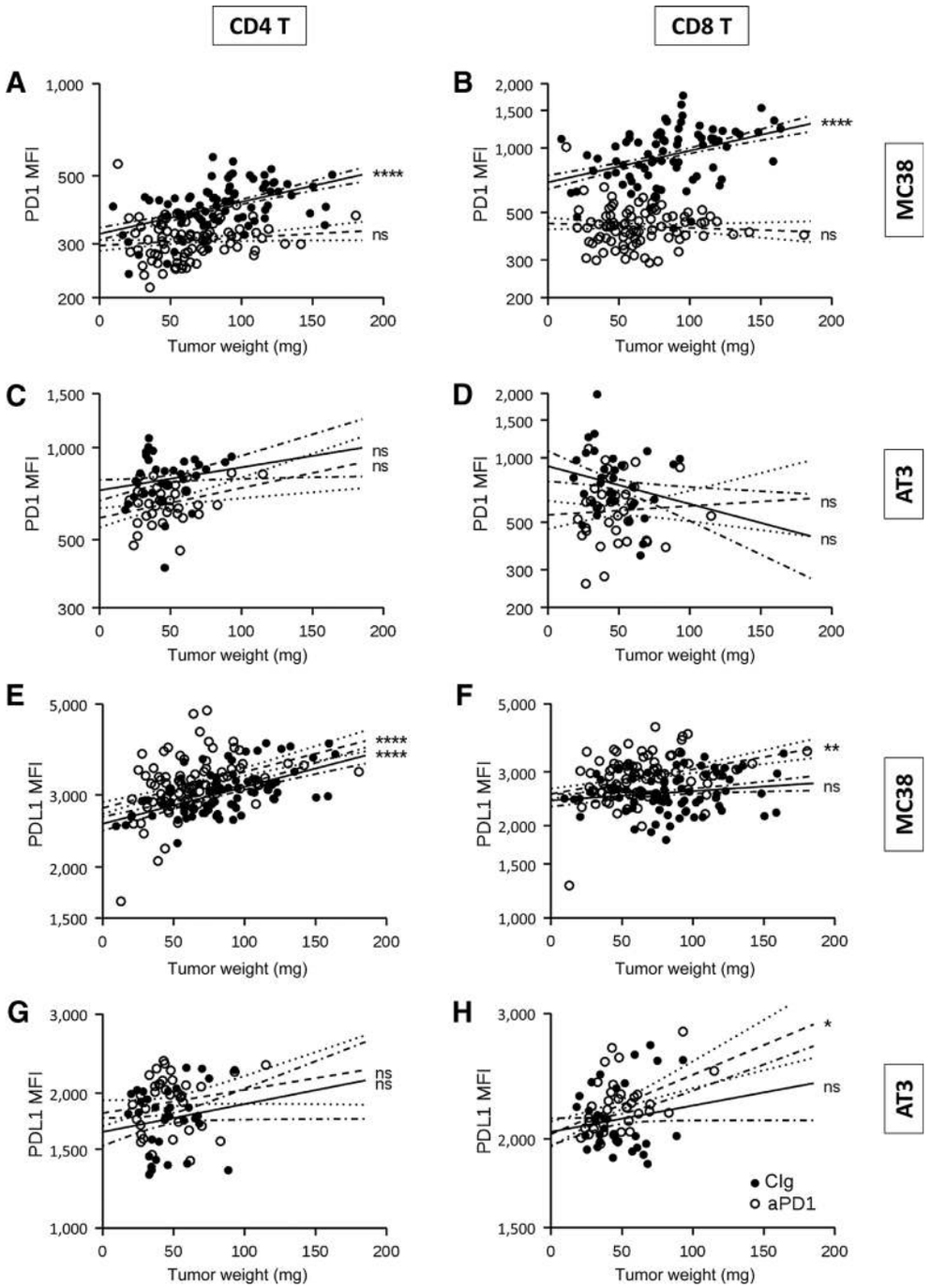

Figure 6.
PD1 MFI on $CD8^+$ T cells predicts tumor aggressiveness and response to anti-PD1 mAb. ANCOVA was applied to test the association between the PDL1 or PD1 MFI on various TIL subsets ($CD4^+$ T, $CD8^+$ T, $CD11b^+/Gr1^+$, $CD45.2^-$) and the tumor weight and the interaction between the two slopes. Plots of PD1 MFI (A–D) and PDL1 MFI (E–H) on $CD4^+$ (left) and $CD8^+$ T cells (right) against the weight of tumors (monitored 2 to 3 days after the first injection of mAb) from mice inoculated with MC38 (A and B; E and F) and AT3 (C and D; G and H) tumor cells and treated with cIg (solid circles) or anti-PD1 mAb (open circles). Solid (cIg) and dashed (anti-PD1 mAb) lines correspond to the slopes and associated SE as estimated by the ANCOVA model for each treatment group. All experiments described in this manuscript comprising $n = 34$ to 36 (AT3) and 79 to 86 (MC38) mice/group were gathered for this analysis. The analyses pertaining to the $CD45.2^-$ and myeloid cell fractions were not significant in this context and therefore not included. (*, $P < 0.05$; **, $P < 0.01$; ***, $P < 0.001$; ****, $P < 0.0001$).

using the combinations of anti-CTLA-4 (Treg-depleting clones) and anti-PD1 mAbs (16, 30); radiotherapy plus anti-CTLA-4/anti-PD1 or anti-CD137/anti-PD1 mAbs (15, 31), anti-VEGF and anti-PD1 mAbs (32) may be partly mediated through Treg depletion or a disruption of Treg suppressive function, leading to reductions in T-cell PD1 levels and frequency. The study of mechanisms of

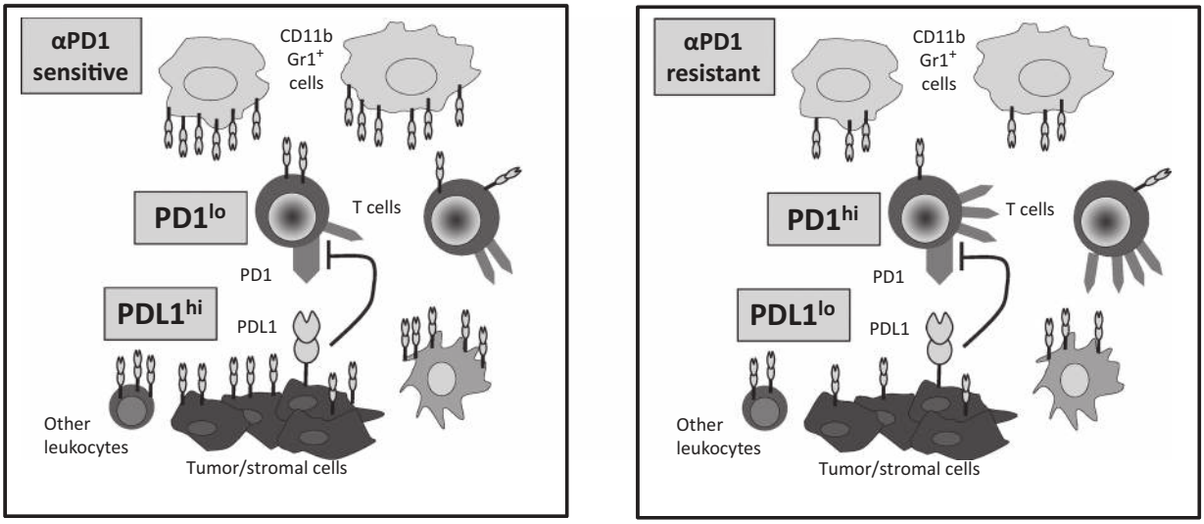

Figure 7.
Schematic diagram of the PD1/PDL1 axis in anti-PD1–sensitive and –resistant tumors. Left, in a tumor microenvironment with $PD1^{lo}$ T cells, an increased level of PDL1 expression is present that increases the probability of PD1 ligation on T cells. Right, in contrast, in a tumor microenvironment with $PD1^{hi}$ T cells, a low level of PDL1 expression is sufficient to ensure the ligation of PD1 on T cells.

Treg regulation of T-cell PD1 expression levels is currently underway.

$PD1^{lo}$ T cells produced higher levels of IFNγ and TNF in comparison to $PD1^{hi}$ T cells, which might in turn induce PDL1 expression in the tumor microenvironment, to shape T-cell PD1 status. From our ANCOVA analyses, the lower level of PDL1 expression on MC38 $CD8^+$ TILs predicted responses to anti-PD1 mAb. With an even lower PDL1 expression on AT3 $CD8^+$ T cells, it is possible that the disruption of a *trans* interaction between $CD8^+$ T cells might explain the efficacy of anti-PDL1 mAb. Interestingly, PDL1 expression on $CD45.2^-$ cells was unchanged upon PD1 blockade, suggesting a minor role for the nonimmune (tumor) cell PDL1 in regulating the PD1/PDL1 axis. Although we uncovered an inverse correlation between T-cell PD1 and immune cell PDL1 expression in the tumor microenvironment, to this point, it remains unclear how the relationship is initiated. Our data suggest that the PD1/PDL1 axis is dynamically regulated according to the changes imposed on PD1 and/or PDL1 in a spatiotemporal manner (Fig. 7).

It is important to note that our findings may apply to tumors where significant T-cell infiltrates are present. It has been recently shown that the vast majority of patients with melanoma with $CD8^+$ TILs present before pembrolizumab (anti-PD1) treatment will respond to therapy. In this light, it is of great interest to now assess whether a dynamic PD1/PDL1 axis exists in patients who first respond to anti-PD1 therapy but eventually relapse (i.e., transition from $PD1^{lo}$ to $PD1^{hi}$). A segregation of "responsive" and "less responsive or resistant" anti-PD1–treated MC38-bearing mice is currently underway to monitor therapeutic efficacy and acquired resistance during anti-PD1 therapy in individual mice. The levels of PD1 and PDL1 may not be predictive when tumors have few T cells present. This is particularly true where oncogenes may be regulating the level of tumor PDL1 expression (9–11). We have reproduced the inability of anti-PD1 to reduce frequencies of PD1-expressing $CD8^+$ T cells in other tumors such as CT26 and Renca. The biology of the intratumor $PD1^-$ $CD8^+$ T cells in the anti-PD1–insensitive AT3 tumor requires further analysis and a study of the mechanisms by which distinct $PD1^-$ and $PD1^{hi}$ $CD8^+$ T-cell populations are generated and a possible *trans* interaction in the AT3 tumor is currently underway.

Given the successes of anti-PD1 mAbs in treating patients with melanoma, renal cell carcinoma, NSCLC, and Hodgkin lymphoma (3–6, 12), PD1 levels and frequencies on the intratumor T cells pre- and posttherapy in these patients should now be assessed. In patients with pembrolizumab-treated NSCLC, Rizvi and colleagues have recently showed that a higher level of nonsynonymous mutation burden in the tumor was associated with improved treatment benefits (33). While the intratumoral PDL1 and T-cell PD1 status was not reported, we reason this study warrants further investigation regarding the association of nonsynonymous mutation burden with the number of $CD8^+$ T cells and their PD1 status. At this stage, there are very few centers, if any, which have a sufficient number of samples collected fresh pre- and post-analysis from patients who have $CD8^+$ TIL and received anti-PD1 therapy but have failed. Using state-of-the-art immunohistochemical (IHC) analysis, Tumeh and colleagues recently reported the importance of intratumoral $CD8^+$ T cells in patients with pembrolizumab-treated melanoma (12). It is however worth noting that multiplex IHC is currently not quantitative enough to determine the critical expression level of PD1 on intratumoral $CD8^+$ T cells; hence, it does not provide insight into PD1 expression/threshold levels on intratumoral T cells. The absence of intratumoral $CD8^+$ T cells is one of the major reasons for anti-PD1 resistance, but our work has demonstrated another mechanism of treatment resistance in tumors despite substantial intratumoral T-cell infiltration.

Disclosure of Potential Conflicts of Interest

M.J. Smyth reports receiving a commercial research grant from Bristol Myers Squibb. No potential conflicts of interest were disclosed by the other authors.

Authors' Contributions

Conception and design: S.F. Ngiow, M.J. Smyth
Development of methodology: S.F. Ngiow
Acquisition of data (provided animals, acquired and managed patients, provided facilities, etc.): S.F. Ngiow, A. Young, L. Zitvogel
Analysis and interpretation of data (e.g., statistical analysis, biostatistics, computational analysis): S.F. Ngiow, A. Young, N. Jacquelot, T. Yamazaki, D. Enot, M.J. Smyth
Writing, review, and/or revision of the manuscript: S.F. Ngiow, A. Young, M.J. Smyth
Administrative, technical, or material support (i.e., reporting or organizing data, constructing databases): S.F. Ngiow, M.J. Smyth
Study supervision: S.F. Ngiow, M.J. Smyth

Acknowledgments

The authors thank Liam Town, Kate Elder, and Joanne Sutton for breeding, genotyping, and maintenance and care of the mice used in this study. They also thank Jeffrey Ravetch for providing the original C57BL/6 FcγR III and FcγR IV gene-targeted breeding pairs and Mark Hogarth for providing the original C57BL/6 FcRγ gene-targeted breeding pairs.

Grant Support

S.F. Ngiow, A. Young, and M.J. Smyth were supported by a National Health and Medical Research Council of Australia (NH&MRC) Australia Fellowship (628623) and Senior Principal Research Fellowship (1078671) and a QIMR Berghofer Ride to Conquer Cancer Grant. A. Young was supported by a Cancer Council Queensland PhD fellowship.

The costs of publication of this article were defrayed in part by the payment of page charges. This article must therefore be hereby marked *advertisement* in accordance with 18 U.S.C. Section 1734 solely to indicate this fact.

Received April 22, 2015; revised July 1, 2015; accepted July 2, 2015; published OnlineFirst July 24, 2015.

References

1. Pardoll DM. The blockade of immune checkpoints in cancer immunotherapy. Nat Rev Cancer 2012;12:252–64.
2. Hodi FS, O'Day SJ, McDermott DF, Weber RW, Sosman JA, Haanen JB, et al. Improved survival with ipilimumab in patients with metastatic melanoma. N Engl J Med 2010;363:711–23.
3. Topalian SL, Hodi FS, Brahmer JR, Gettinger SN, Smith DC, McDermott DF, et al. Safety, activity, and immune correlates of anti-PD-1 antibody in Cancer. N Engl J Med 2012;366:2443–54.
4. Ansell SM, Lesokhin AM, Borrello I, Halwani A, Scott EC, Gutierrez M, et al. PD-1 blockade with nivolumab in relapsed or refractory Hodgkin's lymphoma. N Engl J Med 2015;372:311–19.
5. Hamid O, Robert C, Daud A, Hodi FS, Hwu W-J, Kefford R, et al. Safety and tumor responses with lambrolizumab (anti-PD-1) in melanoma. N Engl J Med 2013;369:134–44.
6. Robert C, Long GV, Brady B, Dutriaux C, Maio M, Mortier L, et al. Nivolumab in previously untreated melanoma without BRAF mutation. N Engl J Med 2015;372:320–30.
7. Powles T, Eder JP, Fine GD, Braiteh FS, Loriot Y, Cruz C, et al. MPDL3280A (anti-PD-L1) treatment leads to clinical activity in metastatic bladder cancer. Nature 2014;515:558–62.
8. Taube JM, Anders RA, Young GD, Xu H, Sharma R, McMiller TL, et al. Colocalization of inflammatory response with B7-h1 expression in human melanocytic lesions supports an adaptive resistance mechanism of immune escape. Sci Transl Med 2012;4:127ra37.
9. Atefi M, Avramis E, Lassen A, Wong DJ, Robert L, Foulad D, et al. Effects of MAPK and PI3K pathways on PD-L1 expression in melanoma. Clin Cancer Res 2014;20:3446–57.
10. Parsa AT, Waldron JS, Panner A, Crane CA, Parney IF, Barry JJ, et al. Loss of tumor suppressor PTEN function increases B7-H1 expression and immunoresistance in glioma. Nat Med 2007;13:84–8.
11. Xu C, Fillmore CM, Koyama S, Wu H, Zhao Y, Chen Z, et al. Loss of Lkb1 and Pten leads to lung squamous cell carcinoma with elevated PD-L1 expression. Cancer Cell 2014;25:590–604.
12. Tumeh PC, Harview CL, Yearley JH, Shintaku IP, Taylor EJM, Robert L, et al. PD-1 blockade induces responses by inhibiting adaptive immune resistance. Nature 2014;515:568–71.
13. Yao S, Zhu Y, Chen L. Advances in targeting cell surface signalling molecules for immune modulation. Nat Rev Drug Discov 2013;12:130–46.
14. Giorgini A, Brown HJ, Lock HR, Nimmerjahn F, Ravetch JV, Verbeek JS, et al. FcγRIII and FcγRIV are indispensable for acute glomerular inflammation induced by switch variant monoclonal antibodies. J Immunol 2008;181:8745–52.
15. Hazenbos WL, Gessner JE, Hofhuis FM, Kuipers H, Meyer D, Heijnen IA, et al. Impaired IgG-dependent anaphylaxis and Arthus reaction in Fc gamma RIII (CD16) deficient mice. Immunity 1996;5:181–8.
16. Nimmerjahn F, Lux A, Albert H, Woigk M, Lehmann C, Dudziak D, et al. FcγRIV deletion reveals its central role for IgG2a and IgG2b activity in vivo. Proc Natl Acad Sci 2010;107:19396–401.
17. Takai T, Li M, Sylvestre D, Clynes R, Ravetch JV. FcR gamma chain deletion results in pleiotrophic effector cell defects. Cell 1994;76:519–29.
18. Kim JM, Rasmussen JP, Rudensky AY. Regulatory T cells prevent catastrophic autoimmunity throughout the lifespan of mice. Nat Immunol 2007;8:191–97.
19. Ngiow SF, von Scheidt B, Akiba H, Yagita H, Teng MWL, Smyth MJ. Anti-TIM3 antibody promotes T Cell IFN-γ-mediated antitumor immunity and suppresses established tumors. Cancer Res 2011;71:3540–51.
20. Verbrugge I, Hagekyriakou J, Sharp LL, Galli M, West A, McLaughlin NM, et al. Radiotherapy increases the permissiveness of established mammary tumors to rejection by immunomodulatory antibodies. Cancer Res 2012;72:3163–74.
21. Curran MA, Montalvo W, Yagita H, Allison JP. PD-1 and CTLA-4 combination blockade expands infiltrating T cells and reduces regulatory T and myeloid cells within B16 melanoma tumors. Proc Natl Acad Sci 2010;107:4275–80.
22. Duraiswamy J, Kaluza KM, Freeman GJ, Coukos G. Dual blockade of PD-1 and CTLA-4 combined with tumor vaccine effectively restores T-Cell rejection function in tumors. Cancer Res 2013;73:3591–603.
23. Sakuishi K, Ngiow SF, Sullivan JM, Teng MWL, Kuchroo VK, Smyth MJ, et al. TIM3+FOXP3+ regulatory T cells are tissue-specific promoters of T-cell dysfunction in cancer. Onco Immunol 2013;2:e23849.
24. Selby MJ, Engelhardt JJ, Quigley M, Henning KA, Chen T, Srinivasan M, et al. Anti-CTLA-4 antibodies of IgG2a isotype enhance antitumor activity through reduction of intratumoral regulatory T cells. Cancer Immunol Res 2013;1:32–42.
25. Simpson TR, Li F, Montalvo-Ortiz W, Sepulveda MA, Bergerhoff K, Arce F, et al. Fc-dependent depletion of tumor-infiltrating regulatory T cells co-defines the efficacy of anti-CTLA-4 therapy against melanoma. J Exp Med 2013;210:1695–710.
26. Bulliard Y, Jolicoeur R, Windman M, Rue SM, Ettenberg S, Knee DA, et al. Activating Fc γ receptors contribute to the antitumor activities of immunoregulatory receptor-targeting antibodies. J Exp Med 2013;210:1685–93.
27. Penaloza-MacMaster P, Kamphorst AO, Wieland A, Araki K, Iyer SS, West EE, et al. Interplay between regulatory T cells and PD-1 in modulating T cell exhaustion and viral control during chronic LCMV infection. J Exp Med 2014;211:1905–18.
28. Kao C, Oestreich KJ, Paley MA, Crawford A, Angelosanto JM, Ali M-AA, et al. Transcription factor T-bet represses expression of the inhibitory receptor PD-1 and sustains virus-specific CD8+ T cell responses during chronic infection. Nat Immunol 2011;12:663–71.

29. Herbst RS, Soria J-C, Kowanetz M, Fine GD, Hamid O, Gordon MS, et al. Predictive correlates of response to the anti-PD-L1 antibody MPDL3280A in cancer patients. Nature 2014;515:563–67.
30. Wolchok JD, Kluger H, Callahan MK, Postow MA, Rizvi NA, Lesokhin AM, et al. Nivolumab plus ipilimumab in advanced melanoma. N Engl J Med 2013;369:122–33.
31. Twyman-Saint Victor C, Rech AJ, Maity A, Rengan R, Pauken KE, Stelekati E, et al. Radiation and dual checkpoint blockade activate non-redundant immune mechanisms in cancer. Nature 2015;520:373–7.
32. Voron T, Colussi O, Marcheteau E, Pernot S, Nizard M, Pointet A-L, et al. VEGF-A modulates expression of inhibitory checkpoints on CD8+ T cells in tumors. J Exp Med 2015;212:139–48.
33. Rizvi NA, Hellmann MD, Snyder A, Kvistborg P, Makarov V, Havel JJ, et al. Mutational landscape determines sensitivity to PD-1 blockade in non–small cell lung cancer. Science 2015;348:124–28.